Using a side-branched volume to tune the acoustic field in a looped-tube travelling-wave thermoacoustic engine with a RC load

Ali Al-Kayiem and Zhibin Yu*

School of Engineering, University of Glasgow, Glasgow, Scotland, United Kingdom

*Corresponding author, E-mail: Zhibin.Yu@glasgow.ac.uk

Abstract

Traveling-wave thermoacoustic engine utilises a compact acoustic network to obtain a right time-phasing between the acoustic velocity and pressure oscillations within the regenerator to force gas parcels to experience a Stirling-like thermodynamic cycle. As such, thermal energy can be converted to mechanical work (i.e., high-intensity pressure waves). It is therefore crucial to control the time-phasing carefully to improve the performance of thermoacoustic engines. Various ways have been proposed and demonstrated for adjusting time-phasing, including both passive and active methods. The aim of this study is to introduce a new passive phase tuning method (i.e., a side-branched acoustic volume) to tune the time-phasing within a looped-tube travelling wave thermoacoustic engine. The proposed concept has been investigated both numerically and experimentally in this research. An experimental rig was simulated and designed using DeltaEC software (Design Environment for Low-amplitude ThermoAcoustic Energy Conversion). It was then constructed according to the obtained theoretical model. The result of this study showed a qualitative agreement between experimental measurement and numerical simulations, demonstrating that the proposed technique can effectively adjust the phase angle between the acoustic velocity and pressure oscillations within the loop-tube thermoacoustic engines, and improve its performance.

***Keywords*:** Phase tuning, Travelling-wave, Thermoacoustic engine, RC load.

Nomenclature

Symbol	Quantity	SI
a	Sound speed	m/s
P	Charging pressure	Pa
p	Acoustic pressure	Pa
T	Temperature	ºC
V	Volume	m^3
ρ	Density	Kg/m^3
ω	Angular frequency	rad/s
C_s	Acoustic compliance	m^3/Pa
$\dot{Q}_{in}$	Input heating rate	W
$\dot{E}$	Acoustic power	W
u	Acoustic velocity	m/s
U	Volumetric acoustic velocity	m^3/s
Z	Normalised acoustic impedance	$Pa.s/m^3$
Θ	Phase angle difference	°
η	Energy efficiency	%
Abbreviation		
AHX	Ambient heat exchanger	
SAHX	Secondary ambient heat exchanger	
HHX	Hot heat exchanger	
REG	Regenerator	
TBT	Thermal buffer tube	
FBP	Feedback pipe	
RC	Resistance – Compliance acoustic load	

1. Introduction

A traveling wave thermoacoustic engine is essentially an acoustic equivalent of a conventional Stirling engine that has a complicated mechanical mechanism to implement the Stirling power cycle. In a travelling wave thermoacoustic engine, when a modulated sound wave propagates through a regenerator from the cold to the hot end, the gas parcels undergo a Stirling-like thermodynamic cycle at a microscopic level due to their complicated interactions between their displacement and heat transfer with solid porous material of the regenerator [1, 2]. Based on this principle, a travelling wave thermoacoustic engine can be built by employing a carefully designed acoustic network to tune the pressure oscillation to be nearly in phase with the velocity oscillation within the regenerator [3, 4]. As such, thermal energy can be converted to mechanical work (i.e., high-intensity pressure waves) at macroscopic level.

A typical traveling-wave thermoacoustic engine includes a pair of ambient and hot heat exchangers, a regenerator, and an acoustic resonator [4]. The regenerator is sandwiched by a pair of hot and ambient heat exchangers, forming a so-called “thermoacoustic core”. The regenerator, similar to that of a conventional Stirling engine, is a section of porous material with high porosity and large number of tiny passages. It is usually made of stainless steel mesh discs in practice. In order to achieve perfect heat transfer between the working gas and the regenerator material, the equivalent pore diameter of those passages within the regenerators are normally a few times smaller than the thermal penetration depth of the working medium under the operating conditions [4]. The hot heat exchanger transfers heat from external heat sources to the working gas within the thermoacoustic engine, while the ambient heat exchanger rejects heat from the working gas to the external heat sink. This pair of heat exchangers establishes and maintains a steep temperature gradient along the axis of

the regenerator to facilitate the Stirling-like thermodynamic cycle process to take place at a microscopic level.

Similar to Stirling engines [5], thermos-fluidic oscillatory engines [6, 7], and two phase reciprocating engines [8, 9], thermoacoustic prime movers are external heat engines and can be powered by all kinds of heat sources (e.g., waste heat sources). Although their working principle is sophisticated, they are simple to build and maintain due to the absence of moving parts, and are environmentally friendly as their working fluids are normally inert gases such as helium or argon.

There have been continuous efforts to develop thermoacoustic engines over the decades [10-16]. Based on the concept of travelling wave thermoacoustic engines proposed by Ceperley [1, 2], Yazaki et al. [3] demonstrated the first lopped-tube traveling wave thermoacoustic engine which, however, only achieved very low energy efficiency because of the large acoustic losses resulting from high acoustic velocity in the regenerator and resonator. To reduce such acoustic losses, Backhaus and Swift [4] later developed a so-called travelling wave thermoacoustic Stirling engine (TASHE). They placed the thermoacoustic core within a torus that has a length much shorter than the acoustic wavelength. The torus consists of an inertance tube, an acoustic compliance volume, and a thermoacoustic engine core, forming a compact acoustic network to obtain a near traveling-wave time-phasing and high local acoustic impedance (i.e., 15–30 times of $\rho_m a/A$) within the regenerator. Hence, much higher energy efficiency has been achieved. Tijani and Spoelstra later designed and built a thermoacoustic Stirling heat engine prototype, and achieved 49% of Carnot efficiency under the same working conditions [17].

In addition to the thermoacoustic core, a resonator is essential and it normally has two main functions: One is to provide a positive feedback mechanism to the thermoacoustic engine core so that the spontaneous acoustic oscillation induced within the thermoacoustic engine can be sustained. For this reason, it is sometimes also called a feedback pipe. The other is to transmit the acoustic power generated within the engine core to acoustic loads [18-20].

One of the key challenges for developing an efficient travelling wave thermoacoustic engine is to accurately control and tune the phase angle between the acoustic pressure and velocity to in-phase travelling-wave condition. In the past decades, various techniques have been developed for controlling and tuning phase in different engines or coolers, including Stirling engines, Stirling coolers, pulse-tube coolers, thermoacoustic engines and coolers.

In conventional Stirling engines and coolers, different mechanical mechanisms involving crank-arms are used to control the motions of pistons and displacers to force the pressure and velocity oscillations are almost in phase within the regenerator [5]. Inertance tubes (i.e., a long and thin tube) have been widely used as phase shifter in pulse-tube coolers to keep oscillating pressure and volume flow rate in phase in the middle of regenerator [6-21]. A gas reservoir is normally attached to the end of the inertance tube to create an open-end acoustic boundary. However, it has also been proposed and demonstrated that an inertance tube can achieve similar phase shifting effects without a reservoir [22-24].

In traveling wave thermoacoustic engines, in order to improve system performance, a variety of techniques have also been proposed and demonstrated to tune the phase angles between pressure and velocity oscillations. Backhaus and Swift employed an inertance tube combined with a compliance volume in their TASHE to obtain a travelling wave phasing within the

regenerator [4]. Gardner and Swift also used an inertance tube in a cascade thermoacoustic engine as a phase shifter [6]. Yu et al. [25] demonstrated a travelling-wave thermoacoustic electricity generator with an ultra-compliant alternator. A side-branched stub has been introduced to match the alternator to the engine. In addition, an ambient heat exchanger was also designed to have low porosity and longer length, to work as a phase shifter. Late, Kang et al. [26] reported a two-stage traveling-wave thermoacoustic generator using two subwoofers as power converters. One was installed within the engine loop which suppressed the Geoden acoustic streaming, while the other was installed at the end of a side-branched pipe. Both a ball valve and the side branched pipe were used to tune the acoustic fields within their system to the optimal conditions. All the above-mentioned methods can be categorised as passive techniques.

In addition to those passive phase tuning methods, active phase tuning techniques have also been investigated. Desjouy et al. [27] proposed an active control of the spatial distribution of the acoustic field by means of auxiliary acoustic sources. Two loudspeakers were installed to the resonator of a looped-tube travelling wave thermoacoustic engine. These two loudspeakers were carefully controlled to produce and emit sound waves into the thermoacoustic engine. As such, the acoustic fields within the engine can be tuned to the optimal conditions to maximise the thermal-to-acoustic energy conversion occurring within the thermoacoustic core. It was reported that the appropriate tuning of the two auxiliary sources could increase the acoustic work production in the engine.

Simplicity is the most mentioned advantage of thermoacoustic engines. Although the active control of acoustic field is very interesting from the theoretical prospective, it is practically not very attractive because it complicates the design and operation of the engine and

introduces extra moving parts. Passive tuning of the acoustic field is apparently more attractive due to its simplicity and absence of moving parts.

According to the literature review above, one can see that the control and optimisation of the acoustic field (particularly the time-phasing) within thermoacoustic engines are critical for improving their efficiency. However, the mechanism of phase tuning has not been fully understood, and remain an interesting subject. It is therefore important to explore new phase tuning methods. Simple, passive and effective phase tuning methods are particularly needed.

This research proposes a new passive phase tuning technique that uses a side-branched variable acoustic volume to tune the phase angle between the acoustic velocity and pressure oscillations in a looped-tube travelling wave thermoacoustic engine. Acoustically speaking, such a volume introduces a parallel acoustic compliance to engine's feedback pipe that is essentially an acoustic waveguide. It can shunt part of the acoustic volumetric velocity away from the feedback pipe at the location where it is installed. As such, it can adjust the local acoustic impedance within the feedback pipe of the engine, subsequently the phase angle between the acoustic pressure and velocity along the engine. In theory, it does not introduce any acoustic resistance and inertance, so it is simple and compact to build and does not consume acoustic power.

In this paper, the function of the proposed phase tuning method is firstly modelled and demonstrated through a series of comprehensive numerical simulations based on DeltaEC software (Design Environment for Low-amplitude ThermoAcoustic Energy Conversion) [28, 29]. An experimental rig is then constructed to demonstrate its function experimentally. The obtained experimental results verify the numerical model qualitatively, and demonstrated that

the performance of the engine can be improved by using a side-branched acoustic volume as a passive phase tuning device.

2. Numerical simulations

Previous research showed that the acoustic velocity tends to be high at some locations along the looped-tube travelling-wave thermoacoustic engine due to the inconsistent cross-sectional area along the engine. A stub was introduced to correct the acoustic field within the looped-tube engine [25]. It was found that the compliance component of the side-branched stub played an important role in improving the performance of the engine, while the acoustic resistance of the stub did not contribute to the phase tuning effect but consumed acoustic power especially when the engine operated at high power level.

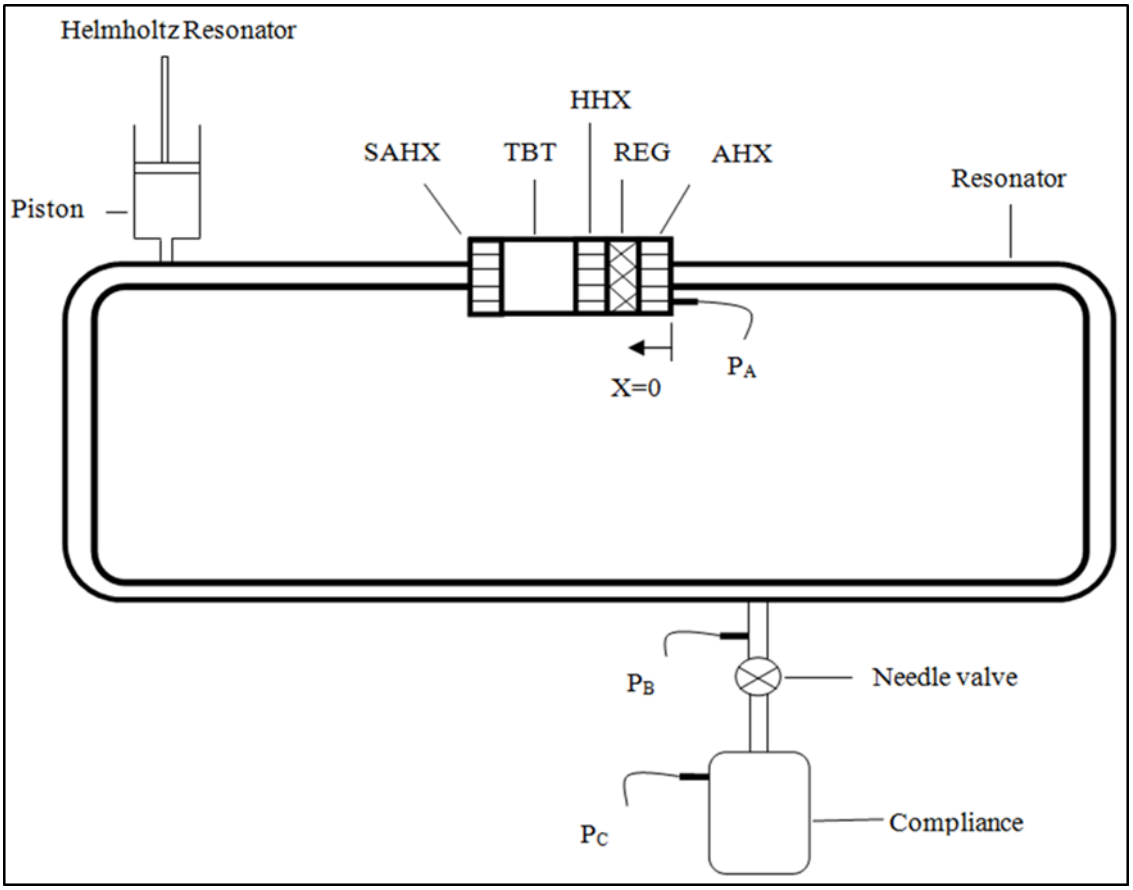

Fig.1. Schematic of the experimental system.

In this paper, a side-branched volume is introduced to the looped engine to tune the phase angle between the pressure and velocity oscillation within the engine. The looped-tube travelling wave thermoacoustic engine was the first implementation of the travelling wave thermoacoustic engine [3]. It has the simplest geometric configuration for constructing travelling wave thermoacoustic engines, and therefore is relatively easy to model. Fig. 1 shows the schematic of the system that is investigated in this research

As shown in Fig. 1, this engine consists of an ambient heat exchanger (AHX), a regenerator (REG), a hot heat exchanger (HHX), a thermal buffer tube (TBT), a secondary ambient heat exchanger (SAHX). In order to evaluate the engine's performance, a RC acoustic load (i.e., a combination of acoustic resistance and compliance [12]) is installed.

From the acoustical point of view, such a side-branched acoustic volume forms a Helmholtz resonator. In theory, it will not consume acoustic power as it only stores acoustic power. Its acoustic compliance C_s is defined as

$$C_s = \frac{V}{\gamma P_m}, \tag{1}$$

where V, P_m and γ are the volume, mean pressure and the ratio of specific heat capacity, respectively [29]. The compliance is varied by changing the size of the side-branched volume in both experiments and simulation.

DeltaEC code has been employed to simulate the present thermoacoustic system. It uses a simplified one-dimensional approximation and assumes that the amplitude of oscillation is

low and has sinusoidal time dependence [28]. The basic mathematic model has been summarised and shown in Appendix A. The design process involves a series of comprehensive simulations. Some typical simulation results are presented in this section to demonstrate the working principle of the rig, as well as the function and effectiveness of the proposed phase tuning device, i.e., the side- branched acoustic volume. The side-branched volume is varied to achieve the maximum acoustic power generated in the engine. To allow the analysis of engine's performance, energy efficiency η is defined as

$$\eta = \frac{\dot{E}_{load}}{\dot{Q}_{in}}, \quad (2)$$

where $\dot{E}_{load}$ is the acoustic power extracted and consumed by the RC load, and $\dot{Q}_{in}$ is the heat power input to the engine via the hot heat exchanger. The working gas is air at atmospheric pressure, and operating frequency is set as around 60 Hz. The heating power is fixed at around 260 Watts in all simulations. The simulation results of the optimised model are summarised and presented in Fig. 2 (a-e).

Figure 2 (a) shows the distribution of the acoustic power flow along the engine. Around 36 W of acoustic power flows into the ambient heat exchanger of the engine core and it is amplified inside the regenerator to around 87 W. The hot heat exchanger, thermal buffer tube, and a section of feedback pipe dissipate around 27W of acoustic power. The acoustic power dissipated by the side-branched Helmholtz resonator is unnoticeable as expected. There is a sharp drop of acoustic power at the location where the RC acoustic load is connected. The RC load extracts around 16 W of acoustic power. The section of feedback pipe between the RC load and the engine core further dissipates around 8 W of acoustic power, and the remaining 36 W acoustic power is fed back to the engine core. The heating power is around 260 W, so the calculated energy efficiency is around 6.1% according to Equation (2).

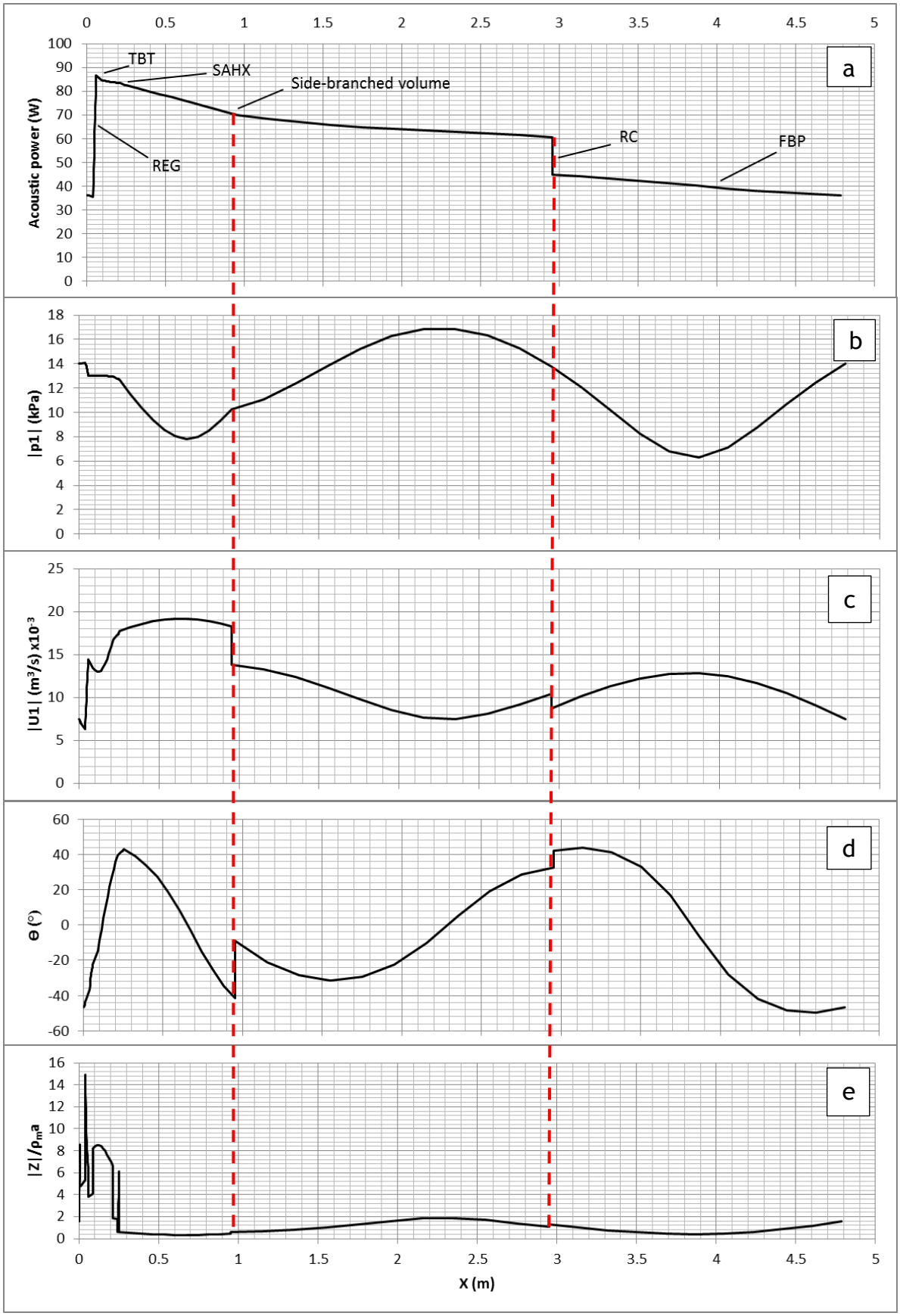
a
Acoustic power (W)
TBT
SAHX
Side-branched volume
REG
RC
FBP
b
|p1| (kPa)
c
|U1| (m³/s) x10⁻³
d
Θ (°)
e
|Z|/ρmᵃ
X (m)

218

Fig. 2. Simulation results of the acoustic field: (a) Acoustic power flow, (b) pressure amplitude, (c) volumetric velocity, (d) phase angle between pressure and velocity, and (e) normalised acoustic impedance.

Figure 2 (b) shows the pressure amplitude distribution along the system. It can be clearly seen that there are two peaks and two troughs of pressure amplitude along the engine loop. One peak appears at the engine core section (i.e., the regenerator and the hot and cold heat exchangers), indicating a high acoustic impedance at this location. The RC load is located close to the other pressure amplitude peak, and the resultant high acoustic impedance could minimise the RC load's effect on the acoustic field within the engine. The maximum and minimum pressure amplitude are around 16.8 and 6.0 kPa along the engine, respectively. The ratio between them is about 2.8. In an ideal travelling wave condition, this ratio should be close to 1. Therefore, it can be inferred that the acoustic field has some standing wave components due to acoustic reflection.

Figure 2 (c) shows the distribution of volumetric velocity along the system. There are two peaks and two troughs along the engine loop. Low volumetric velocity within the engine core is achieved to avoid viscous dissipation within the regenerator and heat exchangers where the flow resistances are high. It can also be seen that the volumetric velocity increases significantly due to the sharp temperature gradient along the regenerator. It should be highlighted that the volumetric velocity decreases sharply at the locations where the side-branched volume (i.e., a Helmholtz resonator) and the RC load are installed, this is mainly due to the shunt of volumetric flow rate to these two components.

Figure 2 (d) shows the phase difference between pressure and velocity oscillations along the engine loop. It clearly shows that the side branched volume significantly changes the phase angle between the pressure and velocity from -40° to about -4°, bringing it towards to the ideal travelling wave condition, i.e., 0°. The RC-load changes the phase angle slightly by around 4°, moving it away from the ideal travelling wave conditions. This Fig. clearly demonstrates that the side-branched volume can effectively adjust the phase angle in the engine.

Figure 2 (e) presents the normalized acoustic impedance along the system. In this model, it can be seen that the normalized acoustic impedance in the most parts of the system is around 1 as expected, and it is around 15 at the engine core section. Usually, the acoustic impedance within the engine core should be in the range 15-30 times that of $\rho_m a$ to reduce the acoustic losses [4]. Therefore, this model has met this requirement.

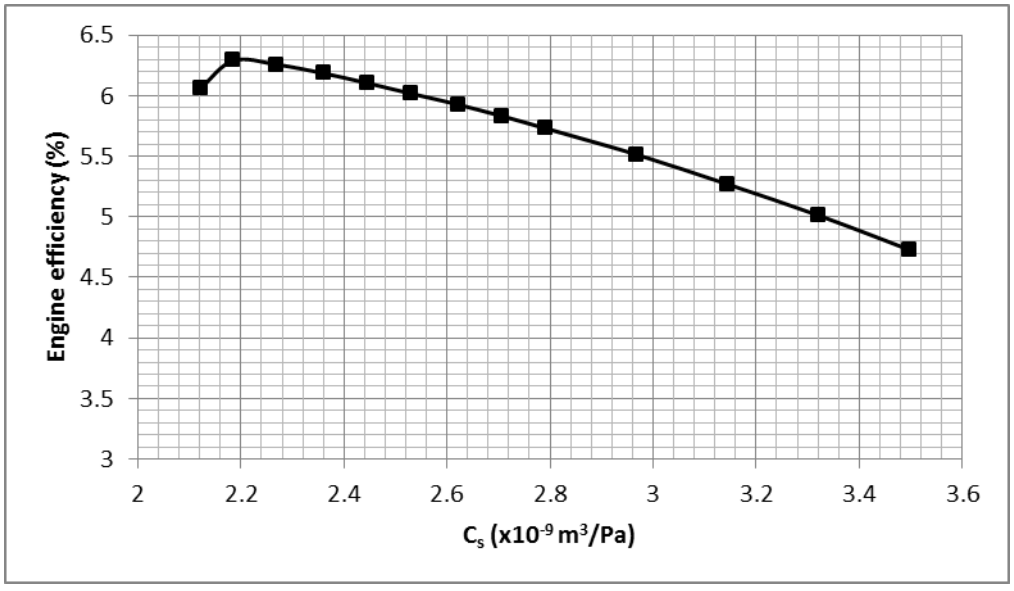

Fig. 3. Optimisation of acoustic compliance Cs for efficiency of the engine.

Figure 3 shows the effect of the side-branched volume on the efficiency of the engine. It can be seen that the acoustic compliance of the side-branched volume has strong effects on the performance of the engine. The efficiency firstly increases, and then decreases with the increase of C_s. There is an optimal value about C_s=2.185x10^{-9} m^3/Pa. It should be noted that C_s=2.185x10^{-9} m^3/Pa was chosen for the optimised model, of which the results are shown in Fig. 2 (a-e).

3. Experimental setup

Based on the optimised model, an experimental rig was then constructed. Fig. 4 shows a photo of the obtained experimental rig. The working gas is air at atmospheric pressure. As shown in both Figs. 1 and 4, this engine consists of an ambient heat exchanger (AHX), a regenerator (REG), a hot heat exchanger (HHX), a thermal buffer tube (TBT), a secondary ambient heat exchanger (SAHX), and a RC acoustic load to extract the acoustic power produced by the engine.

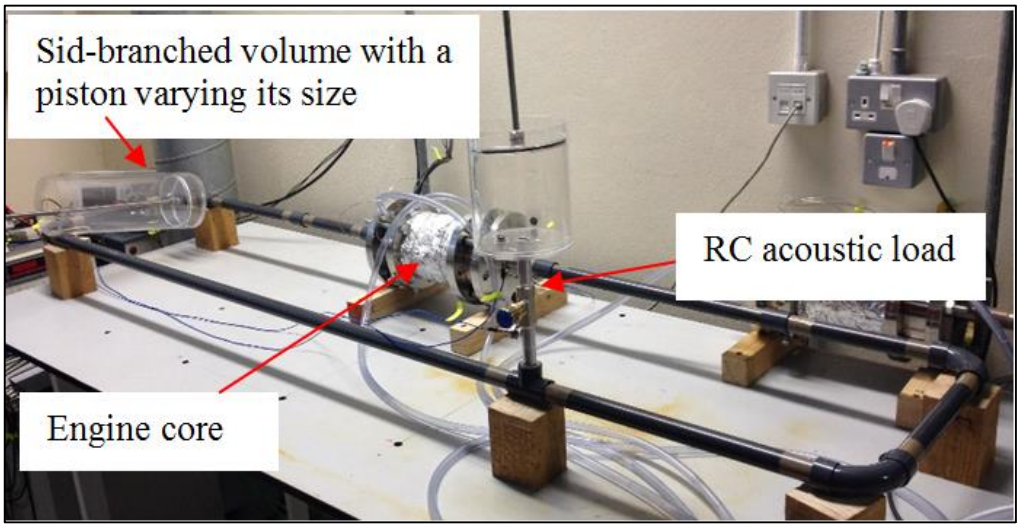

Fig. 4 The photo of the experimental rig.

A side-branched acoustic volume (12.6 cm diameter), whose volume can be varied by changing the position of a piston connects to the looped-tube engine about 70 cm away from the secondary ambient heat exchanger. The volume is connected to the loop through a connection pipe that is 3 cm in length and 2.1 cm in diameter. The total length of the looped tube engine system is around 4.8 m. The diameters of engine core and acoustic resonator are 65 mm and 20 mm, respectively. As the main interest of this research is to demonstrate the function of the proposed phase tuning technique rather than obtaining high power output at high efficiency, atmospheric air is used as working fluid. PVC pipes instead of metal pipe are used as a feedback pipe to minimise the cost.

As shown in Fig. 5 (a), the ambient heat exchanger is made of a cooper block which is 65 mm in diameter and 27 mm long. It is a design that has been widely used in the past [9]. Gas passengers are made of 204 holes (I/D 3 mm) drilled in parallel to the heat exchanger's centreline. Two holes with the diameter of 6mm are drilled perpendicular to the heat exchanger to pass the cooling water. The porosity of the ambient heat exchanger is around 28%.

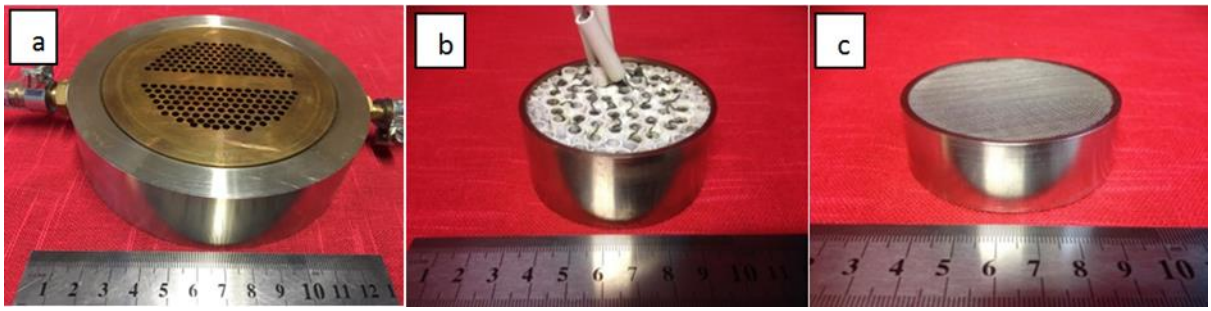

Fig. 5. a) ambient heat exchanger, b) hot heat exchanger, and c) regenerator.

As shown in Fig. 5 (b), the hot heat exchanger is made from Nickel-Chromium resistance wire (NIC-80-020-125). The wire is formed into a coil with a 3.2 mm diameter using 0.51

mm diameter wire. It is inserted inside ceramic tubes to prevent any electrical contact with the metal case. The diameter and length of the HHX are 65 and 30 mm, respectively. The porosity of the hot heat exchanger is around 50%. The length of the ceramic tube is 25 mm, and the outside and inside diameters are 6.4 and 4 mm, respectively. The total resistance of this heater is about 5 Ohms. Electrical power is supplied to the heater at a maximum voltage of 50V (which can be varied in the range of 0-50 V) and a maximum current of 10A from an AC power supply via a feed-through to maintain a good seal.

As shown in Fig. 5 (c), the regenerator is made of stainless steel mesh screen wire disks with a mesh number of 50. The disk diameter is 65 mm. The diameter of the wire and the aperture width are 0.14 mm and 0.375 mm, respectively. In total, 60 mesh disks are placed inside a 20 mm long stainless steel can (1 mm in thickness). The calculated porosity and hydraulic radius is 78.4% and 126.77 μm, respectively.

To reduce the heat loss from the high temperature section of the thermoacoustic engine core to the ambient air, the thermal buffer tube is wrapped with a Ceramic Fibre Insulation Blanket with a thickness of 25 mm. The secondary ambient heat exchanger (SAHX) is identical to the main ambient heat exchanger. The RC load [12, 29] consists of a needle valve (i.e., a RS hydraulic flow control valve 201012) and an acoustic compliance which are connected in series, as shown in Fig. 1. The volume of the acoustic compliance is 1512.8 cm^3. Fig. 5 shows a photo of the experimental rig used in this research.

Three Type-K thermocouples are installed to measure the temperatures at the two ends of the regenerator and within the heater. Three pressure sensors (i.e., PCB PIEZOTRONICS model 112A22) are installed at three different positions as shown by P_A, P_B, and P_C in Fig. 1 to

measure the pressure amplitudes and the phase angles. The phase angles between these signals are measured by a SR830 DSP lock-in amplifier with an accuracy of 0.01°. A data acquisition card has been used to record the signals from the thermocouples and pressure sensors.

4. Experimental results and analysis

The acoustic oscillations start spontaneously in the system when the temperature difference between the cold and hot end of the regenerator exceeds the onset temperature difference around 247 ˚C. The operating frequency of this system is measured as 60.5 Hz which agrees with the simulations. The electric power is fixed as 450 W for all the experiments presented below, which is much higher than 260 W that was set in the simulations in the Section 2.

The acoustic power consumption of the RC load technique is measured using a standard two-sensor method [30, 31]. The pressure amplitude and phases at location P_B and P_C are measured by two pressure transducers. The phase difference between them is measured using a lock-in amplifier. The opening of the needle valve controls the acoustic velocity entering the volume. The optimal opening was obtained experimentally, and kept constant for all measurements in this section. The acoustic power can be calculated using the equation

$$\dot{E}_{load} = \frac{\omega V}{2\gamma p_m} |P_B||P_C| \sin\theta_{BC}, \quad (3)$$

where ω is the angular frequency, V is the volume of the compliance after the needle valve, γ is the ratio of specific heat capacity, p_m is the mean pressure, P_B is the amplitude pressure

before the needle valve, P_C is the amplitude pressure after the needle valve as shown in Fig. 1, θ_{BC} is the phase angle difference between two pressure oscillations.

Fig. 6 shows the effect of the acoustic compliance of the side-branched volume on the pressure amplitude at location P_B. As C_s increases the pressure amplitude firstly increases, and then decreases. The optimal value of C_s is measured as 2.62×10^{-9} m^3/Pa, which is close to the optimal value C_s=2.185×10^{-9} m^3/Pa as predicted in the simulations (see Fig. 3).

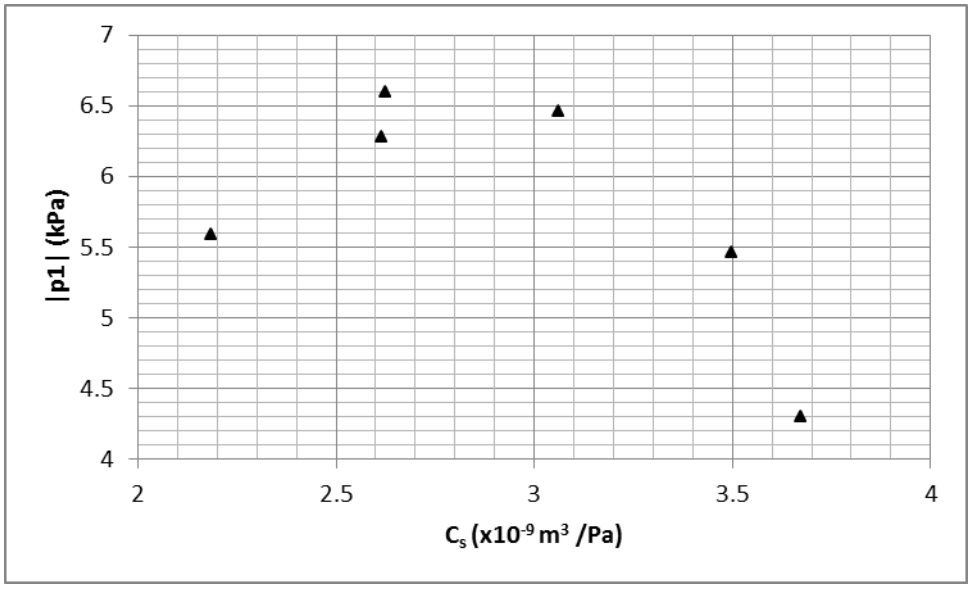

Fig.6. Pressure amplitude at location P_B changes as C_s varies when the heating power is kept as constant.

The side-branched volume has been varied to find out the optimal value of C_s corresponding to the highest acoustic power output and energy efficiency. Fig. 7 shows the relationship between acoustic compliance C_s against acoustic power extracted by the RC load. The measured optimal compliance of the side-branched volume is C_s=$2.62\text{x}10^{-9}$ m^3/Pa, which again is close to the predicted value as shown in Fig. 3.

The experimental results shown in Figures 6 and 7 demonstrate that the side-branched volume can strongly affect the performance of the engine. The measured optimal value of the acoustic compliance of the side-branched volume exists and is close to the predicted optimal value as shown in Fig. 3.

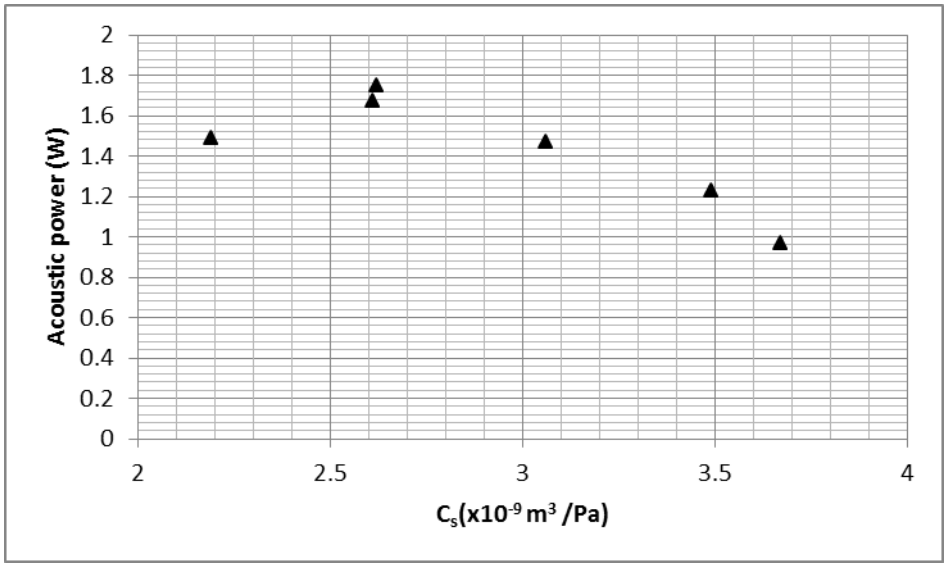

Fig. 7. Acoustic power changes as *Cs* varies when the heating power is kept as constant.

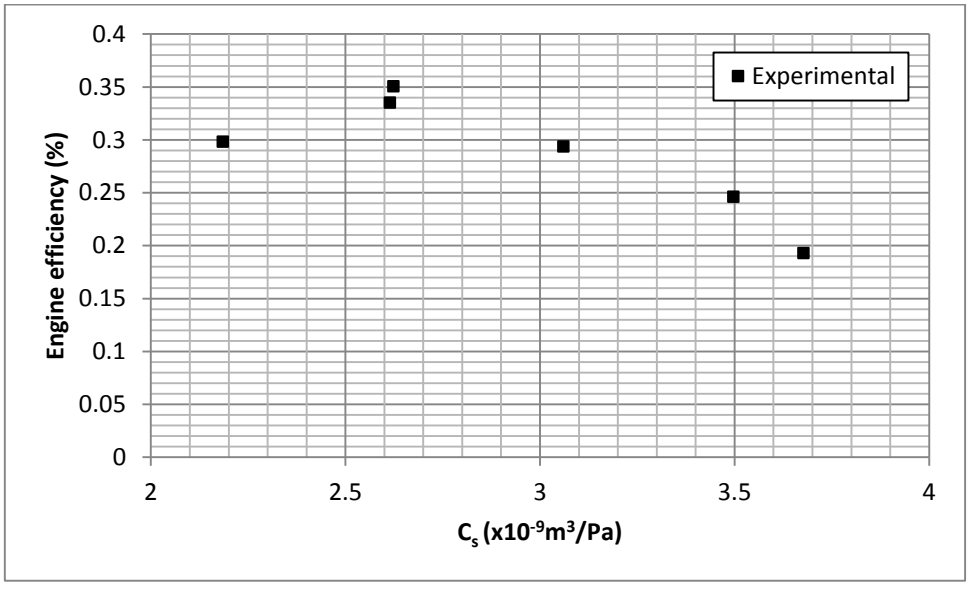

Fig.8. Engine's energy efficiency changes as *Cs* varies when the heating power is kept as constant.

As the heat input power was kept as 450W in the experiments, the energy efficiency of the experimental rig can then be deduced as shown in Fig. 8. The measured energy efficiency is much lower than the predictions as described in the Section 2. Nevertheless, the results in Fig. 8 show a qualitative agreement with the simulations as shown in Fig. 3. Such a qualitatively agreement demonstrates that the side-branched volume can effectively influence the performance of the tested engine.

5. Discussion

Usually, strong acoustic reflection can be induced due to the inconsistent cross-sectional area along looped-tube travelling wave thermoacoustic engines. This can result in relatively higher standing ratio in the acoustic field, consequently higher acoustic velocity at the locations close to the nodes of the acoustic field. High acoustic velocity normally causes high acoustic power losses due to the friction between the working gas and the inner wall of the feedback pipe. Therefore, a logical approach is to reduce the local acoustic velocity without limiting the acoustic pressure.

The numerical simulations have clearly demonstrated the working principle of the proposed phase tuning method. As described in the Section 2, the side-branched volume is essentially a Helmholtz resonator. As shown in Fig. 2 (c), it is connected to the engine at the location where the volumetric acoustic velocity is close to its maximum. It shunts away part of the volumetric velocity from the feedback pipe. It significantly reduces the local volumetric velocity within the feedback pipe (see Fig. 2(c)), but does not affect the local acoustic

pressure (see Fig. 2(b)). As a result, the local phase angle between acoustic pressure and velocity has been significantly improved towards the ideal travelling wave condition, i.e., θ=0 (see Fig. 2(d)). Since a Helmholtz resonator is essentially an acoustic energy storage device, it does not consume acoustic energy (see Fig. 2 (a)). The effectiveness of the proposed phase tuning method has been further demonstrated in the Fig. 3. The acoustic compliance has a strong effect on the engine's performance, and the simulations predict an optimal acoustic compliance C_s=2.185x10^{-9} m^3/Pa, corresponding to the optimal energy efficiency of the engine.

The measured efficiency (0.35%) of the actual engine is much lower than the prediction of 6.1% by the simulations as shown in the Section 2. The onset temperature of this system is about 247 ˚C, which is also much higher than that of the systems tested (around 100 ˚C) in the Ref [25]. There are several possible reasons behind its poor performance. One is the significant heat losses due to insufficient thermal insulation around the hot heat exchanger and thermal buffer tube and acoustic streaming, and the other is the acoustic losses due to the sudden change of the cross-sectional areas along the engine. The PVC pipe and the poor air tightness could also reduce the efficiency due to the leakage of sound waves.

Nevertheless, the main objective of this research is to demonstrate the function of the side-branched volume rather than achiveing high energy efficiency. The experimental results shown in Figs. 6-8 demonstrated that the side-branched volume has a strong effect on the performance of the tested engine. It has also been proven that there exists an optimal acoustic compliance C_s=2.62x10^{-9} m^3/Pa leading to an optimal energy efficiency (see Fig. 8), which is close to the predicted value as shown in Fig. 3. This qualitatively agrees with the numerical simulations.

6. Conclusions

This paper proposes a new method to control and tune the acoustic field within a looped-tube travelling wave thermoacoustic engine using a side-branched volume. From the acoustic point of view, such a side-branched volume is essentially a Helmholtz resonator, and thus does not consume acoustic power. By changing its volume (acoustically speaking, its compliance), we can change the acoustic impedance at the opening of this Helmholtz resonator, and thus adjust the acoustic field within the loop-tubed engine as demonstrated in Fig. 1. It can essentially shunt away part of the volumetric velocity at the low impedance region of the engine so that the acoustic loss can be reduced within the engine.

Based on the simulations, a simple experimental rig using inexpensive components and atmospheric air as working fluid was constructed and tested. Although the measured energy efficiency of the actual experimental rig is much lower than the predictions due to significant heat and acoustic power losses in experiments, there is a qualitative agreement between the simulations and the measurements in terms of the effect of the acoustic compliance of the side-branched volume on the engine's performance. Both the simulations and the experimental results have demonstrated that the proposed side-branched volume can effectively adjust the acoustic field within the looped-tube engine and affect its performance. There is an optimal acoustic compliance corresponding to the best performance in terms of acoustic power output and energy efficiency when the heating power input is fixed.

The future work will focus on building a high efficiency experimental rig using pressurised helium as working fluid to further understand fundamental mechanism of this type of phase

tuning method, and demonstrate and improve its effectiveness.

Acknowledgment

Ali Al-Kayiem would like to acknowledge the finance support from the Ministry of Higher of Education/Babylon University in Iraq (Reference: 553, Iraqi cultural attaché).

Appendix A

According to the linear thermoacoustic theory [28, 29], the thermoacoustic version of momentum and continuity equations can be written as follows:

$$\frac{dp_1}{dx} = -\frac{j\omega\rho_M / A}{1-f_v} U_1 \tag{A1}$$

$$\frac{dU_1}{dx} = -\frac{j\omega A}{\gamma p_M}\left[1+(\gamma-1) f_k\right] p_1 + \frac{(f_k - f_v)}{(1-f_v)(1-\sigma)} \frac{dT_M}{T_M dx} U_1 \tag{A2}$$

The time-averaged acoustic power $d\dot{E}_2$ produced in a length dx of the channel can be written in the complex notation in the general form as

$$\frac{d\dot{E}_2}{dx} = \frac{1}{2}\mathrm{Re}\left[\tilde{U}_1 \frac{dp_1}{dx} + \tilde{p}_1 \frac{dU_1}{dx}\right] \tag{A3}$$

where, "~" indicates a complex conjugate. $\mathrm{Re}[\ ]$ denotes the real part of a complex number.

$$\frac{d\dot{E}_2}{dx} = -\frac{R_v}{2}|U_1|^2 - \frac{1}{2R_k}|p_1|^2 + \frac{1}{2}\mathrm{Re}\left[g\tilde{p}_1 U_1\right]$$

(A4)

where R_v is the viscous resistance per unit length of the channel and it can be written as:

$$R_v = \frac{\omega\rho_m}{A_g}\frac{\mathrm{Im}\left[-f_v\right]}{\left|1-f_v\right|^2}$$

(A5)

$\frac{1}{R_k}$ is the thermal-relaxation conductance per unit length of the channel and it can be written as:

$$\frac{1}{R_k} = \frac{\gamma-1}{\gamma}\frac{\omega A_g}{p_M}\mathrm{Im}\left[-f_k\right]$$

(A6)

while g the complex gain constant for the volume flow rate and it can be written as:

$$g = \frac{\left(f_k - f_v\right)}{\left(1-f_v\right)\left(1-\sigma\right)}\frac{1}{T_M}\frac{dT_M}{dx} \tag{A7}$$

A_g is the cross sectional area of gas channels in the regenerator. Furthermore, $A_g = \phi A$, where ϕ and A are porosity and cross sectional area of the regenerator, respectively.

Equation (A8) quantitatively describes the interaction between the acoustic and temperature fields.

$$\left[1+\left(\gamma-1\right)f_k\right]p_1 + \frac{\gamma p_1}{\omega^2}\frac{d}{dx}\left(\frac{1-f_v}{\rho_M}\right) - \frac{a^2}{\omega^2}\frac{f_k - f_v}{1-\sigma}\frac{1}{T_M}\frac{dT_M}{dx}\frac{dp_1}{dx} = 0 \tag{A8}$$

where, p, U, T, ρ, and γ are the pressure, volumetric velocity, temperature, density and the ratio of specific heat capacities of the gas, respectively; ω and a are the angular frequency

and sound speed of the acoustic wave; f_k and f_v are the spatially averaged thermal and viscous functions, respectively. f_k and f_v are given in [28, 29] in detail. Subscript "1" indicates the first order of a variable, which usually has a complex amplitude.

References

[1] Ceperley PH. A pistonless Stirling engine-The traveling wave heat engine. The Journal of the Acoustical Society of America 1979; 66:1508.

[2] Ceperley PH. Gain and efficiency of a short traveling wave heat engine. The Journal of the Acoustical Society of America 1985; 77:1239.

[3] Yazaki T, Iwata A, Maekawa T, Tominaga A. Traveling wave thermoacoustic engine in a looped tube. Physical Review Letters 1998; 81(15):3128.

[4] Backhaus S, Swift GW. A thermoacoustic-Stirling heat engine: Detailed study. The Journal of the Acoustical Society of America 2000; 107 3148.

[5] Kongtragool B, Wongwises S. Thermodynamic analysis of a Stirling engine including dead volumes of hot space, cold space and regenerator. Renew Energy 2006; 31:345-359.

[6] Gardner DL, Swift GW. Use of inertance in orifice pulse tube refrigerator. Cryogenics 1997; 37(2): 117-121.

[7] Solanki R, Mathie R, Galindo A, Markides CN. Modelling of a two-phase thermofluidic oscillator for low-grade heat utilisation: Accounting for irreversible thermal losses. Applied Energy 2013; 106: 337-354.

513 [8] Markides CN, Smith TCB. A dynamic model for the efficiency optimization of an
514 oscillatory low grade heat engine. Energy 2011; 36: 6967-6980.

515 [9] Christoph JWK, Oyeniyi AO, Aly IT, Andrew JH, Christos NM. A two-phase single-
516 reciprocating-piston heat conversion engine: Non-linear dynamic modelling. Applied
517 Energy 2017; 186(3): 359–375.

518 [10] Backhaus S, Tward E, Petach M. Traveling-wave thermoacoustic electric generator.
519 Applied physics letters 2004; 85: 6.

520 [11] Wang K, Sun D, Zhang J, Xu Y, Luo K, Zhang N, Zou J, Qiu L. An acoustically
521 matched traveling-wave thermoacoustic generator achieving 750 W electric power.
522 Energy 2016; 103: 313-321.

523 [12] Sun D, Wang K, Zhang X, Guo Y, Xu Y, Qiu L. A traveling-wave thermoacoustic
524 electric generator with a variable electric R-C load. Applied Energy 2013; 106: 377–
525 382.

526 [13] Piccolo A. Optimization of thermoacoustic refrigerators using second law analysis.
527 Applied Energy 2013; 103: 358–367.

528 [14] Piccolo A. Design issues and performance analysis of a two-stage standing wave
529 thermoacoustic electricity generator. Sustainable Energy Technologies and
530 Assessments; doi: 10.1016/j.seta.2016.10.011.

531 [15] Yu Z, Jaworski AJ, Abduljalil AS. Fishbone-like instability in a looped-tube
532 thermoacoustic engine. Journal of the Acoustical Society of America 2010; 128(4):
533 188-194.

534 [16] Yu Z, Jaworski AJ. Optimization of thermoacoustic stacks for low onset temperature
535 engines. Proceedings of the Institution of Mechanical Engineers Part A: Journal of
536 Power and Energy 2010; 224(3): 329-337.
537 [17] Tijani MEH, Spoelstra S. A high performance thermoacoustic engine. J Appl Phys
538 2011; 110:093519(1-6).

539 [18] De Blok K. Low operating temperature integral thermo acoustic devices for solar
540 cooling and waste heat recovery. Journal of the Acoustical Society of America 2008;
541 123(5): 3541. And the presentation associated with this paper available on,
542 http://www.aster-thermoacoustics.com.
543 [19] De Blok K, Systemen AT. Multi-stage traveling wave thermoacoustics in practice. In:
544 19th International Congress on Sound and Vibration Vilnius, Lithuania: International
545 Institute of Acoustics and Vibration (IIAV) and Vilnius University 2012; 1-8.

546 [20] De Blok K. Novel 4-stage traveling wave thermoacoustic power generator. In: Paper
547 FEDSM2010-ICNMM2010-30527 in proc ASME 3rd joint US–European fluids
548 engineering summer meeting and 8th international conference on nanochannels,
549 microchannels, and minichannels, Montreal, Canada 2010; August 2–4.

550 [21] Radebaugh R. The development of cryocoolers since 1985. In Proceeding of
551 International Conference on Cryogenics refrigeration, edited by Chen GB et al.,
552 Academic Press, Hangzhou 2003.

553 [22] Luo E, Radebaugh R, Lewis M. Inertance Tube Models and Their Experimental
554 Verification. AIP Conference Proceedings 710, 1485 (2004);doi:10.1063/1.1774842.

555 [23] Dai W, Hu J, Luo E. Comparison of two different ways of using inertance tube in a
556 pulse tube cooler. Cryogenics 2006; 46: 273–277.

[24] Hu JY, Ren J, Luo EC, Dai W. Study on the inertance tube and double-inlet phase shifting modes in pulse tube refrigerators. Energy Conversion and Management 2011; 52(2):1077-1085.

[25] Yu Z, Jaworski AJ, Backhaus S. Travelling-wave thermoacoustic electricity generator using an ultra-compliant alternator for utilization of low-grade thermal energy. Applied Energy 2012; 99:135-145.

[26] Kang H, Cheng P, Yu Z, Zheng H. A two-stage traveling-wave thermoacoustic electric generator with loudspeakers as alternators. Applied Energy 2015; 137: 9-17.

[27] Desjouy C, Penelet G, Lotton P. Active control of thermoacoustic amplification in an annular engine. Journal of Applied Physics 2010; 108: 114904(1-7).

[28] Ward B, Clark J, Swift GW. Design environment for low-amplitude thermoacoustic energy conversion. DELTAEC version 6.2: Users guide. Los Alamos national laboratory; 2008.

[29] Swift, GW. Thermoacoustics: A Unifying Perspective for Some Engines and Refrigerators. New York: Acoustical Society of America; 2002.

[30] Bao R, Chen GB, Tang K, Jia ZZ, Cao WH. Effect of RC load on performance of thermoacoustic engine. Cryogenics 2006; 46: 666–671.

[31] Fusco AM, William CW, Swift GW. Two-sensor power measurements in lossy ducts. J. Acoust Soc Am 1992; 91 (4); 2229-2235.